Functionalization-Dependent Induction of Cellular Survival Pathways by CdSe Quantum Dots in Primary Normal Human Bronchial Epithelial Cells

Amber Nagy,[†] Jennifer A. Hollingsworth,[‡] Bin Hu,[†] Andrea Steinbrück,[‡] Peter C. Stark,[§] Cristina Rios Valdez,[⊥] Momchilo Vuyisich,[†] Michael H. Stewart,[∥] Donald H. Atha,[¶] Bryant C. Nelson,[¶] and Rashi Iyer[#,*]

[†]Bioscience Division, [‡]Center for Integrated Nanotechnologies, Materials Physics & Applications Division, and [§]Chemical Diagnostics and Engineering, Los Alamos National Laboratory, Los Alamos, New Mexico 87545, United States, [⊥]Department of Biochemistry & Molecular Biology, Georgetown University Medical Center, Washington, DC 20007, United States, [∥]Optical Sciences Division, Code 5611, U.S. Naval Research Laboratory, Washington, DC 20375, United States, [¶]Biochemical Science Division, National Institute of Standards and Technology, Gaithersburg, Maryland 20899, United States, and [#]Defense Systems and Analysis Division, Los Alamos National Laboratory, Los Alamos, New Mexico 87545, United States,

ABSTRACT Quantum dots (QDs) are semiconductor nanocrystals exhibiting unique optical properties that can be exploited for many practical applications ranging from photovoltaics to biomedical imaging and drug delivery. A significant number of studies have alluded to the cytotoxic potential of these materials, implicating Cd-leaching as the causal factor. Here, we investigated the role of heavy metals in biological responses and the potential of CdSe-induced genotoxicity. Our results indicate that, while negatively charged QDs are relatively noncytotoxic compared to positively charged QDs, the same does not hold true for their genotoxic potential. Keeping QD core composition and size constant, 3 nm CdSe QD cores were functionalized with mercaptopropionic acid (MPA) or cysteamine (CYST), resulting in negatively or positively charged surfaces, respectively. CYST-QDs were found to induce significant cytotoxicity accompanied by DNA strand breakage. However, MPA-QDs, even in the absence of cytotoxicity and reactive oxygen species formation, also induced a high number of DNA strand breaks. QD-induced DNA damage was confirmed by identifying the presence of p53 binding protein 1 (53BP1) in the nuclei of exposed cells and subsequent diminishment of p53 from cytoplasmic cellular extracts. Further, high-throughput real-time PCR analyses revealed upregulation of DNA damage and response genes and several proinflammatory cytokine genes. Most importantly, transcriptome sequencing revealed upregulation of the metallothionein family of genes in cells exposed to MPA-QDs but not CYST-QDs. These data indicate that cytotoxic assays must be supplemented with genotoxic analyses to better understand cellular responses and the full impact of nanoparticle exposure when making recommendations with regard to risk assessment.

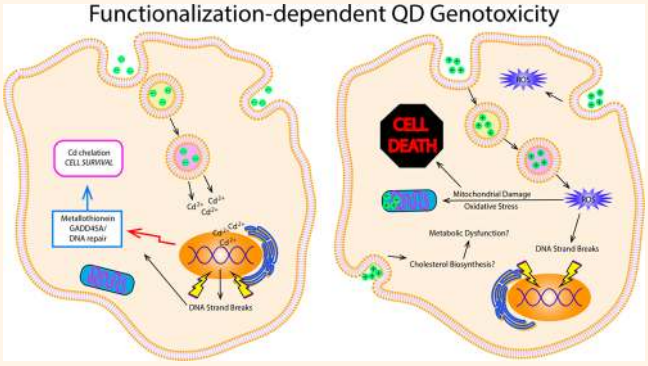

KEYWORDS: genotoxicity · nanomaterials · quantum dots · cytotoxicity · metallothioneins

Engineered nanoparticles are becoming increasingly prevalent in consumer products ranging from computer chips and toner cartridges to solar cells and paint. Semiconductor nanocrystals, or quantum dots (QDs), are of interest to many sectors because of their enhanced optical properties, which are directly correlated to their size. QDs have promise for numerous applications including improving light-emitting devices,[1] solar cells,[2,3] biomedical imaging,[4–6] and therapeutic delivery.[4,7,8]

There is, however, controversy surrounding their safety. Factors including size,[9] charge,[10,11] and surface functionalization[12–15] have been implicated in QD cytotoxicity and cellular responses. Nanoparticle composition can also play a role due to elemental toxicity, especially in the case of selenium or heavy-metal-containing QDs. Both selenium and cadmium toxicity is known,[16–18] and, in the case of QDs, such toxic effects may result from the release of free cadmium ions, for example, in

* Address correspondence to rashi@lanl.gov.

Received for review November 28, 2012 and accepted September 5, 2013.

Published online September 05, 2013
10.1021/nn305532k

TABLE 1. QD Characterization

	absorption max (nm)				
QD type	toluene	water	size from UV−vis (nm)	DLS (hydrodynamic diameter, nm)	zeta-potential (mV)
MPA-QDs	541	541	2.87	4.69 ± 1.03	−55.97 ± 10.94
CYST-QDs	538	532	2.82	3.68 ± 1.14	57.40 ± 16.23

response to oxidative condition or to localization within acidic compartments.[10,19−21] QD cytotoxicity has also derived from formation of reactive oxygen species (ROS) and ensuing oxidative stress.[19,22,23]

DNA damage has been identified in numerous mammalian cell types after exposure to heavy metals, such as Cd, but nanoparticles are also known to induce such effects. For example, silver nanoparticles were found to cause genotoxicity in both alveolar and bronchial epithelial cells,[24,25] and TiO_2 nanoparticles have shown overt genotoxicity in human epidermal cells,[26] liver cells,[27] and alveolar epithelial cells.[28] However, there have been relatively few studies investigating the genotoxic effects of QDs in human cells. *In vivo* studies investigating the genotoxic potential of negatively charged CdSe QDs coated with mercaptoacetic acid in orally challenged mice revealed micronucleus formation in erythrocytes and 8-hydroxy-2-deoxyguanosine (8-OHdG) formation in liver tissue.[29] Further, in intratracheal instilled apolipoprotein E knockout mice, both positively and negatively charged QDs caused significant DNA damage in broncho-alveolar lavage cells.[30] Wang and colleagues[31] found that CdTe QDs induced DNA damage, as indicated by the formation of γH2AX foci in human umbilical endothelial cells, although this damage was reduced in the presence of *n*-acetyl cysteine, an antioxidant, indicating that DNA damage was driven by ROS. Previously, we have established that QD surface charge and functionalization elicit different cytotoxic effects in primary human bronchial epithelial cells (NHBEs).[11] In those studies, positively charged QDs were found to be significantly more cytotoxic than negatively charged QDs; moreover, for the same surface charge but different ligand lengths, we observed variations in the degree of cytotoxicity.

In the current study, to determine the genotoxic potential of QDs, if any, we exposed NHBEs to the CdSe QDs that we previously found to exhibit the *least* cytotoxic potential: small-sized positively and negatively charged CdSe QDs terminated with "short" ligands. In particular, we investigated the role of heavy-metal (Cd) toxicity in the opposed responses. Specifically, we investigated 3 nm CdSe QDs functionalized with mercaptopropionic acid (MPA-QDs), which afforded a negative surface charge, and 3 nm CdSe QDs functionalized with cysteamine (CYST-QDs), which afforded a positive surface charge. Contrary to expectations, the noncytotoxic MPA-QD leached much higher concentrations of Cd^{2+} as compared to the significantly more cytotoxic CYST-QDs. However, both QDs induced notable DNA damage, suggesting that the observed genotoxicity and associated cellular responses might either be Cd-independent or, alternatively, due to the induction of mechanisms that are protective against metal-induced genotoxicity. The latter hypothesis was supported by transcriptional responses in MPA-QD-exposed cells, where we observed a significant increase in the expression levels of 9 genes belonging to the metallothionein gene family and DNA damage/repair genes. On the other hand, the enhanced cellular death observed in CYST-QD-treated cells could be correlated with ROS formation and possibly QD agglomeration. DNA damage, as observed by the comet assay, was confirmed directly by the concentration-dependent appearance of the p53 binding protein 1 (53BP1) and indirectly through Western blot of cytosolic protein targeting p53.

RESULTS

Agglomeration Status of QDs in Biological Media. In all experiments, QDs were suspended in bronchial epithelial cell growth media (BEGM) and added directly to cells. Thus, it is important to understand how biological media components can affect QD stability. MPA- and CYST-QD suspensions were prepared at a concentration of 100 μg/mL. Dynamic light scattering (DLS) was used to measure particle size over time by assessing average sizes for different time points following exposure to BEGM. It is important to note that prior to exposure to BEGM the QDs are stable to agglomeration, and DLS-determined hydrodynamic diameters determined in water are fully consistent with the known particle size plus "thickness" contributions from the organic ligands and the electrical double layer, that is, here, ∼3 nm plus ∼1−2 nm (Table 1). Furthermore, the agglomeration observed following exposure to BEGM can be understood as screening of the electrical double layer repulsion by the added salts, which allows attractive forces to take over and dominate particle−particle interactions. This results in rapid agglomeration as shown in Figure 1, where both MPA-QDs and CYST-QDs achieve sizes >1 μm within 10 min. Above ∼1 μm, DLS values should likely not be considered "quantitatively", but it is nonetheless clear that significant agglomeration takes place and that it is fast for both negatively and positively charged CdSe QDs.

As alluded to above, Table 1 describes the CdSe QDs that were used for this study. The standard hot-injection

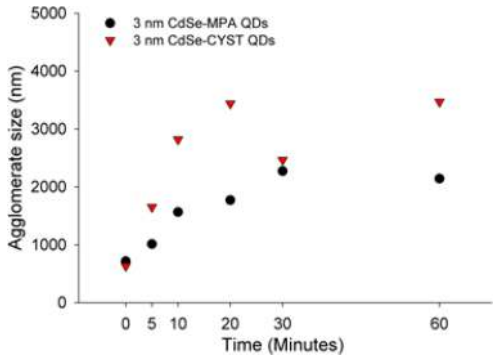

Figure 1. Agglomeration of QDs in cell culture media over time. Each data point represents three independent measurements.

colloidal synthesis method produces uniform QDs approximately 3 nm in diameter. Subsequent ligand exchange with MPA yields negatively charged MPA-QDs, characterized here by a large negative zeta-potential (−55 mV). Cysteamine ligand exchange affords positively charged CYST-QDs and resulted here in a large, positive zeta-potential (>55 mV). In both cases, the large absolute values for zeta-potential indicate high colloidal stability in water. That said, as discussed previously, once exposed to BEGM, electrostatic stabilization fails and the QDs agglomerate. Thus, although we continue to refer to our test materials as MPA-QDs and CYST-QDs, it is important to consider that electrostatically stabilized QDs agglomerate upon introduction to cellular media.

Leaching of Cadmium Ions from QDs in Biological Buffers. In addition to confirming the extent of colloidal instability induced by electrostatic screening effects in high-salt environments (above), we sought to assess the nanocrystal-level stability of the CdSe QD itself. Specifically, we investigated the potential of differently functionalized CdSe QDs dispersed in biological buffers to leach Cd^{2+} ions. We did this using inductively coupled plasma mass spectrometry (ICP-MS, Table 2) to quantitatively determine the amount of free cadmium present following exposure to phosphate buffered saline (PBS) solutions. Percent cadmium losses were calculated as a function of mass and can be found in Supplemental Table 1. After 6 h, 5 or 100 μg/mL MPA-QD solutions in PBS adjusted to a pH of 4 were found to leach 2.16 and 43.52 μg/mL Cd^{2+}, respectively, while the same concentration solutions in pH 7 PBS leached 2.08 and 15.91 μg/mL Cd^{2+}. Note: to ensure that the significant amount of free Cd^{2+} observed for these solutions resulted from Cd^{2+} leaching, rather than excess Cd^{2+} being initially present in the samples, we performed ICP-MS on the starting MPA-QD water solutions adjusted to a concentration of 100 μg/mL. Much lower Cd^{2+} quantities of 3.7 μg/mL were obtained for this control sample, supporting our description of the free Cd^{2+} in the PBS solutions as "leached" ions. As discussed below, the presumed source of leached Cd^{2+} is the oxidation of the MPA thiolate to form dithiol and subsequent release of this now nonbinding form of the ligand from the QD surface, which is known to be further accompanied by controlled Cd^{2+} loss to the solution[32] or uncontrolled QD dissolution.[33,34] The presence of various Cd-binding anions in PBS likely accelerates Cd^{2+} leaching, providing a driving force for solvation that greatly enhances the QD dissolution process.[34]

TABLE 2. ICP-MS Analyses of Cadmium Ion Leaching from QD Suspensions Incubated for 6 h at 37 °C in PBS Buffers Adjusted to pH 4 or 7

		cadmium leached (μg/mL)	
QD concentration (μg/mL)	PBS pH	MPA-QDs	CYST-QDs
5	4	2.16	0.97
100		43.52	1.61
5	7	2.08	0.46
100		15.91	1.88

Also indicative that the observed free Cd^{2+} is not simply a synthetic impurity, for example, but derives from the partial "dissolution" of the QD itself, it was observed that CdSe cores functionalized with sterically bulkier and more protective (but still negatively charged) ligands (mercaptoundecanoic acid (MUA) or poly(ethylene glycol)-appended dihydrolipoic acid (DHLA-PEG-COOH)) leached Cd^{2+} to a lesser extent compared to MPA (Supplemental Table 2). Specifically, at pH 4, where −COOH-terminated ligands are largely protonated and afford relatively poor electrostatic stabilization, both of the bulkier ligands reduce the amount of leached Cd by approximately 20−30% *versus* MPA. More decisively, at pH 7, where the QDs are well-charged, the bulkier ligands show a dramatic decrease in leached Cd from 60% less (MUA) to essentially no observed leaching (DHLA-PEG-COOH). In the latter case, in addition to steric protection, the use of the bidentate (dithiol as opposed to single-thiol) anchoring group improves binding to surface cadmium, inhibiting ligand loss and subsequent release of cadmium.[35,36] Thus, the protective nature of surface ligands depends on both the ligand makeup and the chemical environment, for example, pH. Both 5 and 100 μg/mL CYST-QD solutions in PBS were also subjected to leaching studies. Interestingly, both pH 4 and 7 CYST-QDs were found to leach relatively little Cd^{2+}: 0.97 and 1.61 μg/mL Cd^{2+}, respectively, at pH 4 and 0.46 and 1.88 μg/mL Cd^{2+}, respectively, at pH 7.

It is not necessarily obvious why the negatively charged CdSe QDs exhibit significant leaching, while their positively charged counterparts do not. If we are correct in assuming that Cd^{2+} loss results from oxidation-induced ligand loss followed by Cd^{2+} dissolution or, in the least, a more-exposed QD surface that is susceptible to, for example, phosphate-induced Cd^{2+} "etching", then there appears to exist a fundamental difference in the manner by which the carboxyl-terminated

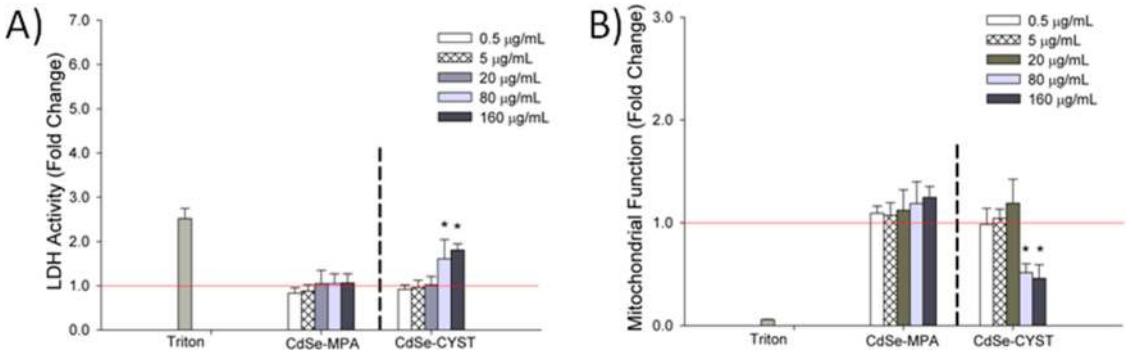

Figure 2. Cytotoxicity of CdSe QDs in NHBE cells is charge-dependent. (A) NHBE cells were exposed to increasing concentrations of negative (MPA) or positive (CYST) CdSe QDs for 24 h prior to assessing cell necrosis using lactate dehydrogenase (LDH) activity as an indicator of cell viability. Cells exposed to 0.1% Triton-100 served as the assay positive control. Experiments were performed in quadruplet on three independent occasions. Significant differences in fold change between exposed cells and media controls (red baseline) are denoted with *; $p < 0.001$. Error bars represent one standard deviation. (B) NHBE cells were exposed to increasing concentrations of CdSe QDs harboring a negative (MPA) or positive (CYST) charge for 24 h. Cellular viability was determined by using water-soluble tetrazolium dye (WST-1) as an indicator of mitochondrial function. Cells exposed to 0.1% Triton-100 served as the assay positive control. Experiments were performed in triplicate on three independent occasions; error bars represent one standard deviation. Significant differences in fold change between exposed cells and media controls (red baseline) are denoted with *; $p < 0.005$.

MPA and the amine-terminated CYST ligands serve to "protect" their QD surfaces from either oxidation or simple etching. We suspect that the sterically bulkier carboxyl end group of the MPA ligand packs relatively poorly compared to the more compact amine, which allows CYST to better cover QD surface sites. Further, amines are capable of hydrogen bonding, which may also help to afford a tighter, more protective ligand layer. It has been shown previously that differences in ligand packing influence the rate of dot dissolution in water.[33]

Effects of QD Functionalization on Cellular viability. Figure 2A revealed a significant ($p < 0.001$) concentration-dependent increase in NHBE necrosis upon exposure to CYST-QDs for 24 h. MPA-QDs (up to 160 μg/mL) did not cause any changes in membrane permeability after either 24 or 48 h of exposure (Supplemental Figure 1). Comparatively, positively charged CYST-QDs were found to be approximately 2-fold more cytotoxic than the negatively charged MPA-QDs. Figure 2B revealed that, when NHBE cells were incubated with CYST-QDs, a significant decrease ($p < 0.005$) in mitochondrial function was apparent for high concentrations (80 and 160 μg/mL) relative to media controls. No significant changes in mitochondrial function occurred when NHBE cells were exposed to MPA-QDs at any of the concentrations tested.

Induction of Intracellular ROS as a Function of QD Charge. NHBE cells were incubated with CdSe MPA- and CYST-QDs for up to 120 min, and intracellular ROS was measured using the fluorescent probe 5-(and-6)-chloromethyl-2′,7′-dichlorodihydrofluorescein diacetate (CM-H_2DCFDA) at 10 min intervals. A significant ($p < 0.005$) dose-dependent increase in ROS was revealed for cells incubated with CYST-QDs (Figure 3). Higher concentrations (80 and 160 μg/mL) induced ROS at levels greater than the H_2O_2 positive control. MPA-QDs did not induce significant ROS at any of the concentrations tested (Figure 3).

DNA Damage (Strand Breaks and Micronuclei Formation). Images of DNA damage associated with strand breaks were analyzed by fluorescence microscopy and showed slight dose−response increases in the length of the comet tails (Figure 4A). The alkaline comet assay revealed a significant ($p < 0.0001$, Figure 4B) increase in oxidative DNA damage in NHBE cells after exposure to CdSe QDs as analyzed by comparison of tail DNA percentage as a quantitative parameter. A statistically significant ($p < 0.0001$) induction in DNA damage was observed at different concentrations of negatively charged MPA-QDs (20 and 160 μg/mL—noncytotoxic concentrations) and positively charged CYST-QDs (0.5 and 20 μg/mL, also noncytotoxic concentrations) after 24 h exposure as compared with untreated (media-only) cells. Cells treated with 250 μmol/L H_2O_2 for 1 h were used as a positive control and exhibited DNA damage in a similar pattern as MPA- and CYST-QDs. However, the negatively charged MPA-QDs (20 μg/mL) appeared to induce a slightly higher, albeit statistically insignificant, increase in strand breaks compared to CYST-QDs.

The formation of micronuclei was quantified to further assess genotoxicity of QDs. While the number of micronuclei increased in response to QD exposure, these changes were not statistically significant compared to media controls. Representative images of micronuclei formation for treatments can be found in Supplemental Figure 2.

Confirmation of QD-Dependent DNA Damage. Immunoblotting of cytoplasmic fractions from NHBE cells exposed for 24 h revealed a decrease in cytoplasmic expression of p53 for treated cells, which is in agreement with a p53-mediated mechanism of DNA damage and repair (Figure 5).

DNA damage induced by QDs was also monitored by the presence of nuclear foci as a result of increased

expression of 53BP1. Immunocytochemistry revealed a significant increase in foci in response to both MPA- and CYST-QDs. Figure 6 quantifies the mean number of 53BP1 foci per cell and also representative 53BP1 images captured after 24 h of exposure.

Corresponding nuclear staining to confirm nuclear localization of 53BP1 foci are found in Supplemental Figure 3. Statistical analyses revealed significant differences in average number of 53BP1 foci per cell when comparing media controls and cells exposed to 20 and 100 μg/mL MPA-QDs ($p < 0.01$ and $p < 0.001$, respectively) and also significant differences in average number of 53BP1 foci per cells between media controls and CYST-QDs for all three concentrations (0.5, 20, and 100 μg/mL, $p < 0.02$, $p < 0.001$, and $p < 0.001$, respectively). Cells incubated with MPA or CYST alone (no QDs) revealed no significant differences in 53BP1 foci, indicating that free ligand is not a major component driving DNA damage (Supplemental Figure 4).

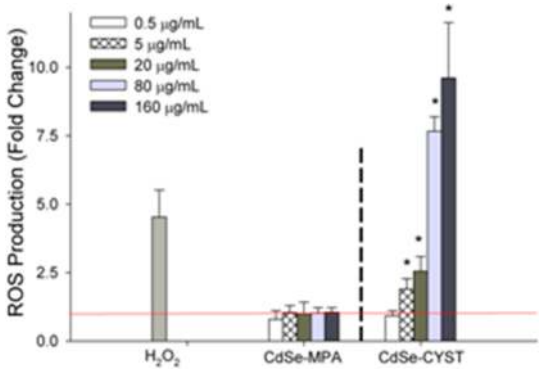

Figure 3. Positively charged CdSe QDs induce significant reactive oxygen species formation in NHBE cells. NHBE cells were exposed to increasing concentrations of CdSe QDs harboring a negative (MPA) or positive (CYST) charge for a total of 120 min (readings were taken every 10 min). Intracellular reactive oxygen species was quantified using the fluorescent probe CM-H_2DCFDA. Cells exposed to 250 μmol/L H_2O_2 served as the positive control. Experiments were performed in triplicate on three independent occasions; graphed data are from the 60 min time point. Significant differences in fold change between exposed cells and media-only controls (red baseline) are denoted with *; $p < 0.01$. Error bars represent one standard deviation.

Negative and Positive QDs Cause Changes in NHBE Gene Expression. High-throughput quantitative real-time PCR (qPCR) was used to measure changes in expression of a targeted panel of genes known to play a role in xenobiotic responses. This panel was chosen to include common, well-characterized gene targets that are associated with stress response, DNA damage repair, inflammation, and mitochondrial function; a complete list of targets and associated function can be found in Supplemental Table 3. Cells were exposed to MPA-QDs and CYST-QD (10 or 100 μg/mL concentrations) for 6 h. Genes which regulate DNA repair, BRCA1 and BRCA2, were downregulated (−1.29-fold and −1.43-fold, respectively) in cells exposed to 10 μg/mL CYST-QDs (Table 3, left panel). At higher concentrations, changes in gene regulation are much more apparent. Downregulation

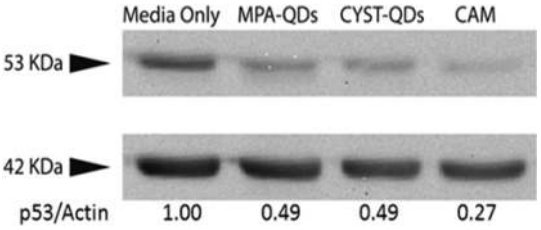

Figure 5. Cytoplasmic p53 is reduced in response to QD exposure. NHBE cells were incubated with 100 μg/mL of MPA- or CYST-QDs for 24 h, and cytoplasmic protein was harvested and assayed for the presence of p53. Ratios are relative to actin loading controls. Camptothecin (CAM, 8 μmol/L), a known inducer of p53-mediated DNA damage, was used as a positive control.

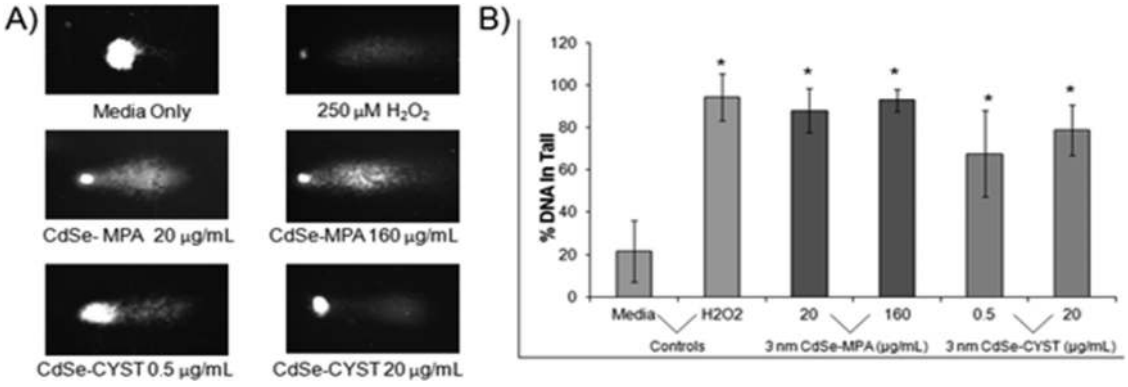

Figure 4. Significant DNA strand breaks are evident in NHBE cells after exposure to negative and positive CdSe QDs. (A) DNA damage (strand break) detection in NHBE cells exposed to CdSe QDs using fluorescence microscopy after staining with SYBR Green I. Characteristic comet shape resulting from increased mobility of the fragmented nuclear DNA is evident after exposure to both negative (MPA) and positive (CYST) CdSe QDs. Images are representative single cells of control groups (media-only and H_2O_2-exposed cells) and QD-exposed cells. (B) Comet assay was used to quantify DNA damage (strand breaks). Data are expressed as percent of DNA in tail for QD-exposed NHBE populations compared to media-only and H_2O_2 (250 μM) controls. Values are presented as mean ± one standard deviation of triplicate slides. Error bars represent one standard deviation ($n = 30$). Significant differences between exposed cells and the media control are denoted with *; $p < 0.0001$.

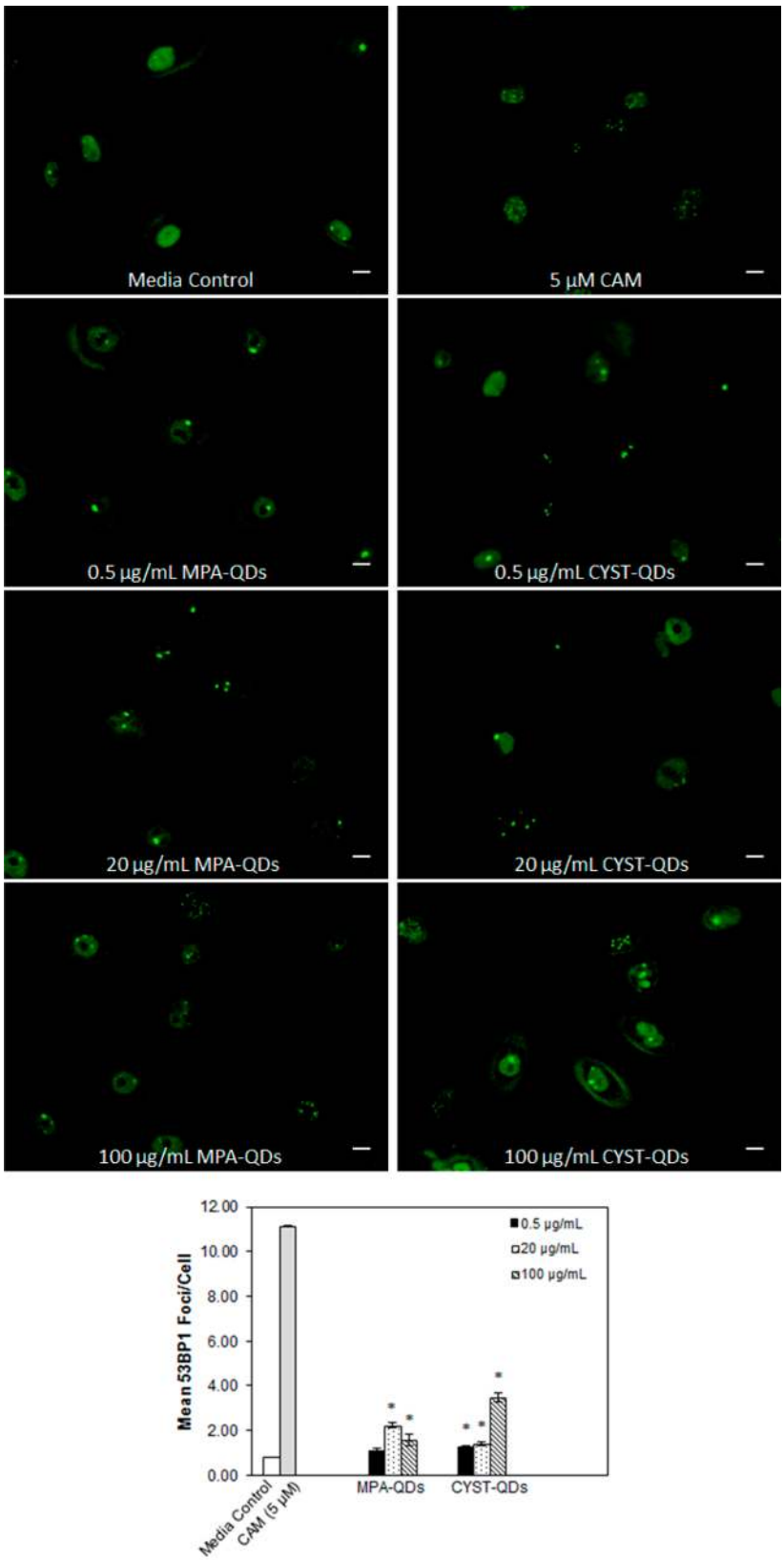

Figure 6. Significant concentration-dependent increases in 53BP1 foci expression. NHBE cells were incubated with MPA-QDs or CYST-QDs at increasing concentrations for 24 h. Bright green foci are indicative of 53BP1 bound to DNA undergoing repair. Scale bars are 5 μm. Mean number of 53BP1 foci per cell for three experimental replicates scoring the number of foci in at least 50 cells per experimental slide. Error bars are one standard deviation, * indicates $p < 0.02$. Images are representative of three experimental replicates.

TABLE 3. Changes in NHBE Gene Expression in Response to Negative (MPA) and Positive (CYST) CdSe QDs Relative to Media Control (Uncertainties Are ± One Standard Deviation)

		gene expression (fold change)			
		10 μg/mL, 6 h		100 μg/mL, 6 h	
cell response pathway	gene	MPA-QDs	CYST-QDs	MPA-QDs	CYST-QDs
DNA damage	CDK1	1.03 ± 0.04	−1.19 ± 0.04	−1.32 ± 0.21	−1.89 ± 0.33
	GADD45A	1.22 ± 0.08	1.21 ± 0.01	2.26 ± 0.15	2.83 ± 0.06
DNA repair	BRCA1	−1.08 ± 0.05	−1.29 ± 0.10	−1.68 ± 0.08	−2.00 ± 0.31
	BRCA2	−1.11 ± 0.05	−1.43 ± 0.12	−2.33 ± 0.20	−1.25 ± 0.23
transcription factor	AP1S1	1.04 ± 0.03	−1.08 ± 0.04	1.44 ± 0.05	−1.61 ± 0.04
	FOS	−1.50 ± 0.33	−1.57 ± 0.15	−1.07 ± 0.03	−2.49 ± 0.18
	TP53	1.14 ± 0.11	−1.13 ± 0.01	1.09 ± 0.13	1.05 ± 0.14
cytokines and chemokines	CXCL1	1.23 ± 0.08	1.06 ± 0.11	3.19 ± 0.09	1.18 ± 0.23
	IFNA1	−1.25 ± 0.17	1.09 ± 0.07	−1.45 ± 0.17	1.80 ± 0.29
	IL1B	1.01 ± 0.03	1.02 ± 0.04	2.33 ± 0.03	2.36 ± 0.06
	IL6	1.43 ± 0.24	1.15 ± 0.13	5.56 ± 0.70	7.25 ± 1.47
	IL8	1.11 ± 0.25	1.16 ± 0.13	2.50 ± 0.23	3.42 ± 0.59
mitochondrial function	CYP1B1	−1.04 ± 0.02	1.28 ± 0.07	1.66 ± 0.08	5.34 ± 0.31

of BRCA1 (−2.00-fold) and BRCA2 (−1.25-fold) was revealed after exposure to 100 μg/mL of CYST-QDs; however, both genes are also downregulated (−1.68-fold and −2.33-fold, respectively) after exposure to 100 μg/mL MPA-QDs (Table 3, right panel). GADD45A, a protein associated with DNA damage, was significantly upregulated in response to both MPA (2.26-fold) and CYST-QDs (2.83-fold) at 100 μg/mL, while CDK1, also involved with DNA damage, was downregulated in exposed cells. The proinflammatory cytokines interleukin-1B (IL-1B), interleukin-6 (IL-6), and interleukin-8 (IL-8) were all upregulated in response to QDs but to a greater extent in cells exposed to CYST-QDs (Table 3, right panel). The CYP1B1 gene was unchanged in NHBE cells incubated with MPA-QDs but was upregulated (5.34-fold) in response to CYST-QDs. The transcription factor c-FOS was downregulated after exposure to either MPA- or CYST-QDs (−1.50-fold and 1.57-fold, respectively) at low concentrations, compared to media controls (Table 3, left panel). While p53 protein expression was found to decline in the cytoplasmic protein fraction of exposed cells, TP53 gene expression was not significantly altered in any of the exposure conditions (Table 3).

Although qPCR is a valuable tool for investigating changes in gene expression, it is difficult to gain a global understanding of transcriptional responses. Therefore, we conducted a more comprehensive analysis of the complete human transcriptome using RNA sequencing technology. A total of 118 genes were significantly changed (52 genes affected by MPA-QD exposure and 66 genes affected by CYST-QD exposure) in response to QD exposure (10 μg/mL for 6 h). Of these 118 genes, there were 8 genes in common among the treatments (Figure 7).

Our panel of qPCR targets was found to directionally agree with the transcriptome data (if qPCR indicated upregulation, the transcriptome data did, as well), although the relative changes were slightly different. Genes that were significantly affected by QD treatment can be found in Supplemental Tables 4 and 5. Interestingly, for cells exposed to MPA-QDs, a significant increase in gene expression of metallothioneins was revealed (levels ranging from 3-fold to over 1000-fold, Table 4), whereas cytochrome P450 genes were upregulated (2−3-fold) in response to CYST-QDs.

DISCUSSION

Semiconductor QDs are increasingly considered as active materials for next-generation solar cells and light-emission technologies. Their multiplexing capabilities, reduced photobleaching, and size tunability also make them attractive candidates for biomedical applications including imaging and therapeutic delivery. While selenium toxicity is indeed an important factor to consider at very high doses (>400 μg), it has also been shown to have protective roles and can enhance DNA repair. As such, we chose to quantify cadmium leaching in our system because of overwhelming evidence associated with cadmium-induced pulmonary carcinogenesis, driven by cadmium-associated inhibition of DNA repair mechanisms and aberrant gene expression. Because inhalation is a common route of particulate and chemical exposure, and also often used as a strategy for drug delivery, we investigated the cytotoxic and genotoxic potential of CdSe QDs in primary NHBE cells. Although it is known that addition of a non-Cd-containing semiconductor, such as ZnS, as a shell onto the CdSe core can significantly reduce the release of Cd^{2+} ions from the QD, we chose to focus our study on CdSe cores. Significantly, even core/shell QDs are subject to similar dissolution processes observed here for the CdSe cores, which could

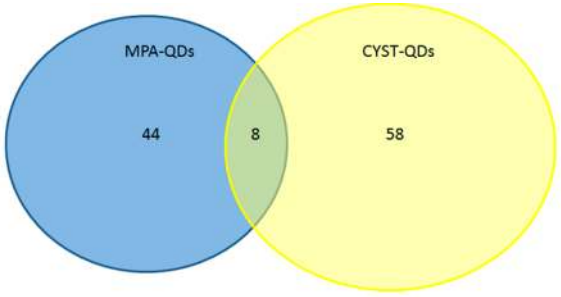

		MPA-QDs *versus* Media Control			CYST-QDs *versus* Media Control		
Gene ID	Gene Symbol	Fold Change	p value	q value	Fold Change	p value	q value
XLOC_000447	GADD45A	2.03	7.18E-06	4.97E-03	1.96	3.88E-10	9.31E-07
XLOC_002244	PGBD5	3.95	2.29E-05	1.20E-02	4.36	8.44E-09	9.03E-06
XLOC_002894	DKK1	0.46	3.40E-05	1.68E-02	0.55	3.00E-06	1.57E-03
XLOC_009490	MT1E	4.00	0.00E+00	0.00E+00	0.52	1.27E-09	2.25E-06
XLOC_011503	ZNF750	3.00	9.25E-05	3.72E-02	2.32	2.22E-05	8.10E-03
XLOC_014647	CYP1B1	0.34	8.44E-05	3.48E-02	3.55	0.00E+00	0.00E+00
XLOC_018216	VGLL3	2.37	1.48E-06	1.16E-03	1.73	1.55E-06	8.95E-04
XLOC_018450	TNFSF10	2.02	1.65E-05	9.59E-03	1.74	1.81E-06	9.83E-04

Figure 7. Common genes affected by QD treatment. NHBE cells were exposed to 10 μg/mL MPA-QDs or CYST-QDs for 6 h prior to RNA isolation and transcriptome analysis using the RSeq platform.

TABLE 4. Metallothionein Gene Family Members Are Upregulated in Response to MPA-QDs

gene ID	gene	function	fold change	*P* value	*Q* value
XLOC_009493	MT1A	metallothionein, binds heavy metals	636.3	1.31×10^{-16}	3.23×10^{-13}
XLOC_009495	MT1B	metallothionein, binds heavy metals	>1000.0	1.15×10^{-6}	9.92×10^{-4}
XLOC_009490	MT1E	metallothionein, binds heavy metals	4.0	0.00×10^{0}	0.00×10^{0}
XLOC_009496	MT1F	metallothionein, binds heavy metals	16.7	0.00×10^{0}	0.00×10^{0}
XLOC_009962	MT1G	metallothionein, binds heavy metals	174.8	0.00×10^{0}	0.00×10^{0}
XLOC_009497	MT1H	metallothionein, binds heavy metals	210.1	0.00×10^{0}	0.00×10^{0}
XLOC_009489	MT1L	metallothionein, binds heavy metals	4.5	3.66×10^{-14}	7.93×10^{-11}
XLOC_009491	MT1M	metallothionein, binds heavy metals	289.4	0.00×10^{0}	0.00×10^{0}
XLOC_009499	MT1X	metallothionein, binds heavy metals	3.7	0.00×10^{0}	0.00×10^{0}

also lead to exposure to the Cd-containing interior. Furthermore, simple CdSe QDs effectively represent a "worst case scenario", allowing us to explore more directly how ligand nature and charge can impact the accessibility of the QDs and their "contents" to the living cells, thus facilitating the ultimate goal to establish the understanding necessary for ranking the toxic potential of nanomaterials. We submit that such an approach would potentially provide guiding principles for the design of more biocompatible nanomaterials without compromising functionality. Our previous work[11] revealed that QDs functionalized with shorter ligands (MPA and CYST) appear to elicit less cytoxicity in NHBE cells, compared to their more cytotoxic counterparts, CdSe QDs functionalized with MUA (negatively charged) and amino-undecanethiol (AUT, positively charged). Thus, the studies presented here were performed using these less cytotoxic CdSe QDs and focused upon the impact of charge and the role of Cd in the observed toxicity. Further, as most studies focus solely on cytotoxicity as a quantifiable end point, we investigated the genotoxic potential of these nanomaterials, a more subtle, yet equally important consequence of nanomaterial exposure, which is often overlooked.

While most nanoparticle characterization (*e.g.*, zeta-potential and size measurements) occurs in water, this is not an accurate portrayal of physiologically relevant biological systems. We therefore performed a time-course study to understand the agglomeration status of MPA- and CYST-QDs in BEGM so we could gain insight into how agglomerate size impacts cytotoxicity. Although BEGM does not exactly replicate the environment

of the bronchial airway, it does contain growth factors and other physiologically relevant biomolecules that have the potential to form a protein corona around the QDs, a phenomenon which is likely to occur when QDs encounter mucin in the respiratory tract. Although DLS data cannot be used to definitively quantify CdSe agglomerate sizes above 1 μm, there is still evidence that agglomeration and differences in agglomeration kinetics can affect QD/cell interactions, including uptake mechanisms and downstream end points such as gene regulation and severity of cytotoxicity. Previous studies have suggested that nanomaterial size dictates cytotoxicity, where smaller QD cores caused increased toxicity.[9,21] However, these studies did not account for agglomeration of QDs in biological media but rather focused on the hydrodynamic diameter of the QDs. In the present study, the core size of the QDs was 3 nm, but the particles agglomerated very quickly (<10 min) upon introduction to BEGM, and it was, in fact, the largely agglomerated CYST-QDs which exhibited greater cytotoxicity in NHBE cells. These data indicate that parameters other than hydrodynamic size dictate cytotoxicity. Others[37] have reported that nanoparticle agglomeration and charge influence uptake rate, subcellular distribution, and potentially cytotoxicity; however, these responses were dependent on cell type and nanomaterial composition. Thus, it stands to reason that factors such as charge and agglomeration potential should be considered when investigating nanomaterial exposure scenarios, biocompatibility, and safety.

The work presented in this article supports the hypothesis that nanomaterial surface functionalization can influence cytotoxicity. In our case, positively charged CYST-QDs (80 and 160 μg/mL) were found to increase necrosis nearly 2-fold compared to negatively charged MPA-QDs at the same concentration. This increase in necrosis was correlated with the production of ROS and supports previous studies where QD cytotoxicity was found to be proportional to oxidative stress.[19,23,38] CYST-QDs were found to induce a concentration-dependent increase in ROS, a response that is well-established to induce a variety of intracellular pathways that ultimately lead to both cyto- and genotoxicity.[39] Treatment of cells with the antioxidant *n*-acetyl cysteine (NAC) postexposure did not rescue the cells, which was in agreement with our previous experiments.[11] However, when cells were pretreated with NAC and then exposed to either MPA-QDs or CYST-QDs, the number of 53BP1 foci was reduced in both cases, but the observed decrease did not reach statistical significance (data not shown). Our data indicate that ROS does not directly cause cytotoxicity, although it may play a role in the genotoxic effect of QDs.

Although MPA-QDs did not cause cytotoxicity in NHBE cells, we sought to uncover if other subtle cellular responses, such as DNA damage, occurred in response to QD exposure. In mouse inhalation studies, QDs were found to cause greater DNA damage as compared to carbon-based and gold nanoparticles.[30] Using comet assays to evaluate DNA damage, we found that MPA-QDs and CYST-QDs caused significantly more DNA strand breaks compared to media-only treated cells. This result was duplicated in NHBE cells exposed to even the lowest concentration of CYST-QDs (0.5 μg/mL). Curiously, while we observed significant DNA damage in response to both the positively and negatively charged QDs, only the positively charged QDs cause cytotoxicity. This unexpected, but notable, DNA damage response from MPA-QD treated cells contradicted the high cell viability observed in these cells. To understand this anomaly, we investigated how the transcriptional responses might differ between the two treatments.

We found changes in expression of genes commonly known to counter DNA damage and also those involved with cell cycle checkpoints. In agreement with our DNA damage cellular data, GADD45A, a stress-induced gene directly related to DNA damage and response, was found to be upregulated in NHBE cells after exposure to 100 μg/mL of MPA- or CYST-QDs. Upregulation of GADD45A expression has been directly correlated to G2/M arrest under stress (excess Zn) in NHBE cells[40] and by DNA-damaging agents. The gene expression data also indicate that other genes involved with cell cycle checkpoint control, such as CDK1, are modulated in response to QD exposure. At low concentrations (10 μg/mL) of CYST-QDs and high concentrations (100 μg/mL) of both MPA- and CYST-QDs, we found that BRCA1 and BRCA2 were downregulated. Downregulation of BRCA1 is commonly associated with sporadic breast cancer[41] as well as pancreatic cancer.[42] Further, it has been implicated in the development of chemotherapeutic resistance by disrupting mitotic spindle checkpoints.[43] Downregulation of BRCA1 has been associated with genetic instability through several mechanisms including anomalies in centrosome duplication, defects in the DNA damage repair, and dysfunctional S phase, G2/M, and spindle checkpoints.[44] Both the positively and negatively charged QDs downregulated CDK1 gene expression at high concentrations, indicating that cells may be compensating for DNA damage by arresting at the G2 checkpoint.[45] Studies have reported downregulation of CDK1 protein and mRNA levels following DNA damage in human cells. Repressed CDK1 expression is only observed in cells with functional p53, implicating a role for p53 in the observed genotoxic and cellular responses.[45] Additionally, decreased levels of p53 protein expression were observed in cytoplasmic fractions of exposed cells. We were able to confirm DNA repair sites through immunocytochemistry specific to 53BP1, a major component of the p53 DNA repair complex. Collectively, these results provide support for the DNA damage induction by the QDs *via* a p53-dependent mechanism; however, further mechanistic studies to

identify the exact role of p53 in DNA damage and repair associated with QD exposure are ongoing in our laboratories.[46] It was also noted that gene expression of CYP1B1 was increased by greater than 5-fold in cells exposed to CYST-QDs, while it was unchanged in MPA-QD-exposed cells. CYP1B1 is a member of the cytochrome P450 superfamily of monooxygenases enzymes, which catalyze many reactions involved in drug metabolism and synthesis of cholesterol, steroids, and other lipids. It is a heme-thiolate monooxygenase capable of metabolizing xenobiotics, such as polycyclic aromatic hydrocarbons (PAHs)[47] and endogenous compounds (*e.g.*, estrogen, testosterone).[48] Apart from its role in xenobiotic metabolism, CYP1B1 is implicated in the bioactivation of pro-carcinogens.[49]

Since the more targeted gene analysis did not offer a reasonable rationale for the observed lack of correlation between cytotoxicity and genotoxicity results in the MPA-QD treated cells, we performed a global transcriptomic analysis using RNA-Seq. Accordingly, NHBE cells were exposed to a genotoxic but not cytotoxic QD concentration (10 μg/mL for 6 h). In total, 118 genes exhibited modified expression levels. Of considerable interest was the significant increase in the expression of the metallothionein family of genes (MT1A, MT1B, MT1E, MT1F, MT1G, MT1H, MT1L, MT1M, and MT1X) for cells exposed to MPA-QDs, which was not apparent in the transcriptome data of CYST-QD-exposed cells. Upregulation of metallothionein gene expression correlated well with our ICP-MS data, which revealed increased Cd leaching from MPA-QDs compared to CYST QDs. Early studies by Derfus *et al.*[20] investigated the cytotoxicity of CdSe QD cores capped with mercaptoacetic acid, which are slightly shorter than the MPA-capped QDs used in our study. In that work, the authors demonstrate that oxidation of the CdSe cores results in increased Cd^{2+} release from the QDs. Non-oxidized QDs were not found to be toxic to cells after a 24 h exposure, while air and UV-exposed QD samples were found to induce massive cytotoxicity, depending on the duration of oxidative conditions. They further went on to correlate the amount of free Cd with cytotoxicity of primary hepatocytes in non-oxidized samples as well as air and UV-exposed QDs, where the addition of protective shells and protein coating (BSA) were able to circumvent some of the cytotoxic effects, likely because longer ligands protect the QD cores from oxidation. In the present study, we revealed a cell-protective mechanism in response to ligand-dependent Cd leaching from our QDs, which appears to promote cell survival. The early work put forth by Kirchner *et al.*[21] also compared the cytotoxic effects of several types of modified QDs, including MPA (which we also used), a ZnS shell, QDs embedded in silica or embedded in a polymer shell. The concentration of Cd^{2+} on the QD surface was calculated and correlated with cytotoxicity, as measured by decreased cell attachment. While we did not observe the cytotoxic responses reported in the studies described above (performed with different cell types), but rather a potential cell-protective mechanism, it appears that different cell types might respond differently to Cd exposure in a manner that is dependent on the degree and pattern of metallothionein expression. *In vivo* studies comparing intra- and interspecies genetic variability suggest that differences in MT expression may influence the susceptibility of rats or mice to lung carcinogenesis induced by inhalation of Cd compounds.[50] Moreover, studies have shown that increased metallothionein expression protects cells from apoptotic cell death, which might explain the lack of cytotoxicity observed in the negatively charged CdSe QDs.[51] Our MT expression data are in agreement with King-Heiden *et al.*,[52] who also correlated increased Cd release from QDs with upregulation of metallothionein in zebrafish. Further, negatively charged (capped with MUA) QD cores were found to leach more Cd compared to shelled QDs and were also found to cause gross cytotoxicity in macrophages and human bronchial epithelial cells in addition to causing mortality in a zebrafish model.[53] However, it should be noted that our previous data[11] have indicated ligand-dependent cytotoxic differences, where cytotoxicity was observed with MUA-capped CdSe QDs but not the MPA-capped QDs used in the current study.

The data presented here indicate a possible mechanism of genotoxicity and cellular compensation strategies upon exposure and dissolution of negatively charged QDs. It is unfavorable for Cd to remain unbound for an extended period as it has a strong affinity for the sulfhydryl groups present in thiols such as reduced glutathione and other cysteine-containing proteins. This affinity can be used to explain perhaps both the DNA damage and cell-protective responses observed in our study, where the genotoxic effect of QDs may be a result of oxidative stress caused by damage due to exhausted antioxidant protein function upon Cd^{2+} interaction. The upregulation of metallothioneins and affinity of Cd^{2+} to the sulfhydryl moieties on these proteins may sequester this Cd in an unavailable form, allowing for repair of DNA damage and survival. A study by Oberdörster *et al.*,[54] comparing Cd-induced inflammatory response in mice *versus* rats, concluded that the differences in lung metallothionein expression between species after inhalation of Cd provide different degrees of sequestration of Cd and consequently protection from its effects. However, in the case of CYST-QDs, oxidative stress may occur independent of Cd leaching, where the cells are unable to recover from oxidative DNA damage resulting in cell death. While transcriptome data did not reveal obvious changes in signaling pathways or any other kind of compensatory survival mechanism in response to CYST-QD exposure, CYST-QDs appeared to modulate genes involved with metabolism and cholesterol biosynthesis. Interestingly, CYP1B1, which catalyzes reactions involved in cholesterol

synthesis, is increased over 5-fold in the CYST-QD-treated cells as observed by qRT-PCR analysis. This is of itself a novel finding worthy of further investigation that may provide insight into the cytotoxic mechanism of CYST-QDs, perhaps uncovering how positively charged QDs adversely affect cell metabolism.

In the present study, both negatively charged and positively charged QDs induced an inflammatory response in NBHE cells upon QD exposure, although CYST-QDs upregulated common proinflammatory cytokine gene expression to a greater extent. This is in agreement with other studies,[55,56] which demonstrated significant inflammation in mouse lungs upon treatment with cadmium-containing QDs. The prolonged activation of a proinflammatory response can cause DNA damage itself, which further complicates matters in terms of understanding the mechanism of nanomaterial cytotoxicity.

We have shown that both QD types induce severe DNA damage in exposed NHBE cells, although negatively charged QDs were not found to be cytotoxic. The comparative enhanced cytotoxicity induced by the positively charged QDs compared to the negatively charged QDs might be a function of their uptake by the cells. Indeed, studies by Chau *et al.*[57] have demonstrated that QD charge dictates the pathway of particle traversal within a tissue, with positively charged QDs doing so intracellularly and negatively charged QDs following a paracellular mechanism. This charge-based fundamental difference in cell/QD interaction and uptake underscores the potential for differing cytotoxic mechanisms due to QD functionalization, although the authors of that study did not report cytotoxic data. It is tempting to reason that negatively charged MPA-QDs elicit cell responses and DNA damage through soluble Cd released from QDs, whereas CYST-QDs cause more potent toxic effects because they have greater propensity to enter cells directly; however, further studies are required to confirm this hypothesis, which are beyond the scope of the current work.

CONCLUSIONS

We propose that MPA-QDs induce DNA damage as a result of Cd^{2+} leached from QD cores. NHBE cells then respond by upregulating metallothioneins which potentially bind these ions, reducing Cd bioavailability, allowing for DNA repair and survival. While NHBE cells exposed to CYST-QDs generate a large ROS response, one which may be responsible for the DNA damage induced, we propose that NHBE cells are unable to mount a sufficiently protective metabolic and antioxidant response to CYST-QDs and succumb through necrotic mechanisms.

MATERIALS AND METHODS

QD Preparation and Characterization. Cadmium oxide (CdO, 99.95%) and oleic acid (90%) were purchased from Alfa Aesar (Ward Hill, MA, USA), 1-octadecene (ODE, 90%), tetramethylammonium hydroxide (TMAH), and cysteamine (CYST, 95%) from Acros Organics (Geel, Belgium), oleylamine (tech grade), mercaptopropionic acid (MPA), and selenium pellet (≥99.999%) from Aldrich (St. Louis, MO, USA), trioctylphosphine (TOP, 97%) and trioctylphosphine oxide (TOPO, 90%) from Strem (Boston, MA, USA). All chemicals were used without any further purification.

CdSe (3 nm) QDs were synthesized as previously described.[11] Briefly, cadmium oleate was prepared by heating 1.45 g of CdO in 20 mL of oleic acid at 170 °C until colorless and cooled to 100 °C prior to degassing under a vacuum. Then 3.95 g of Se (pellet) was dissolved in 50 mL of TOP in an inert atmosphere glovebox to generate the TOP-Se solution.

In an air-free environment, 1 g of TOPO, 8 mL of ODE, and 0.75 mL of cadmium oleate were combined. The reaction mixture was thoroughly degassed at room temperature and again at 80 °C. Temperature was increased to 300 °C under an atmosphere of ultra-high-purity argon. A solution of 4 mL of TOP-Se, 3 mL of oleylamine, and 1 mL of ODE was quickly injected into the cadmium oleate solution. The temperature was subsequently lowered to 270 °C for 1 min to control CdSe QD growth.[58] The reaction was then cooled, yielding CdSe QDs with a diameter of 3 nm.

QDs were purified to remove excess ligands/reactants from the chemical synthesis and excess ligands following transfer to the aqueous phase as described previously,[11] with the addition of several cycles of centrifugation−filtration (Millipore 50 000 MWCO or Amicon Ultra15 30 000 MWCO centrifugal filter unit) following the isopropyl-alcohol-mediated precipitation from water. QD concentrations were calculated according to Yu *et al.*[59] on the basis of UV−vis absorbance spectra. MPA was added to the toluene solution in amounts equivalent to 2 times the number of moles of CdSe and incubated for 2 h. To facilitate the transfer of QDs from organic phase to water phase, a solution of TMAH in water (4 times the number of moles of CdSe) was added dropwise. The water phase was precipitated with isopropyl alcohol, followed by centrifugation (~5 min at 5000 rpm). The resulting pellet was redispersed in distilled water. The procedure for exchange with CYST was essentially the same with the exception that a 20-fold excess of CYST was used, and acid rather than base was used to promote transfer into the aqueous layer. Once the QDs transferred, the pH of the solution was brought back to ~6. Aggregates were carefully removed by centrifugation.

QD Characterization. The agglomeration properties of QDs in biological media were investigated by dynamic light scattering (DLS) on suspensions of QDs over time using a Malvern Zetasizer. Briefly, QD suspensions of 100 μg/mL were made using BEGM cell culture media, and QD size was measured over time up to 1 h. Aqueous suspensions of QDs were also evaluated for size and charge.

Inductively Coupled Plasma Mass Spectrometry (ICP-MS). To understand the stability of QDs in biological buffers, we quantified cadmium core leaching using ICP-MS. In these experiments, either 5 or 100 μg/mL suspensions of QDs were prepared using phosphate buffered saline that had a pH of 7 or 4 to represent cytoplasmic compartments or acidic organelle compartments in the cell. These suspensions were then centrifuged at 485 000*g* for 2 h (Sorvall WX Ultra Series (Thermo Scientific) outfitted with a SW 60 Ti (Beckman Coulter)). Supernatants were assessed for absorbance to ensure that no residual QDs remained in the supernatant and stored at 4 °C until ICP analysis. Samples were quantitatively analyzed for cadmium by ICP-MS using either a Thermo Scientific Element 2 (Thermo Scientific, West Palm Beach, FL) or a Perkin-Elmer Sciex Elan 6100 (Perkin-Elmer Life and Analytical Sciences Shelton, CT) instrument. The analysis method used was based on Method 6020A of the U.S. Environmental Protection Agency's (EPA's) Test Methods for Evaluating Solid Waste: Physical/Chemical Methods (SW-846).

The instruments were calibrated using three concentrations of NIST-traceable standards, and the calibration was verified using a standard from a source independent from the calibration standards. An internal standard of indium was added to all blanks, standards, and samples to compensate for instrument drift.

Cell Culture and QD Exposure. Normal human primary bronchial epithelial cells (NHBEs) were purchased from Lonza (Walkersville, MD, USA) and propagated in bronchial epithelial cell growth media (BEGM, Clonetics Bullet Kit Lonza, Walkersville, MD, USA) on 100 mm Petri dishes coated with type I 50 μg/mL rat tail collagen (BD Biosciences, Bedford, MA, USA) diluted in Dulbecco's phosphate buffered saline (DPBS). Cells were passaged weekly and fed by replacing spent media with fresh media every 2−3 days. For necrosis, apoptosis, reactive oxygen species production, and mitochondrial function assays, cells from passages 3−7 were seeded at 2.5×10^4 cells per well in 96-well flat bottom tissue culture plates and acclimated overnight. Coverslips coated with rat tail collagen were situated in 6-well plates, seeded with 5.0×10^4 NHBE cells per coverslip, and acclimated overnight before exposure to QDs. For comet assays, RNA and protein isolation, cells were seeded at 1.5×10^5 cells per well in 6-well tissue culture dishes. Cells were allowed to acclimate prior to QD exposures. QD suspensions ranging from 0.5 to 160 μg/mL and appropriate controls were prepared in DPBS or BEGM and immediately added to aspirated wells (200 μL/well for 96-well plates and 2 mL/well for 6-well plates). While we report our data as μg/mL of QDs added to the cells, these concentrations equate to 0.3 to 97.0 μg/cm^2 (96-well plates) and 0.1 to 33.3 μg/cm^2 (6-well plates). Cells were incubated for 6 or 24 h in a humidified atmosphere at 37 °C and 5% CO_2 during QD exposures.

Cell Viability Assays. Upon completion of QD exposure, cells were analyzed for necrosis using lactate dehydrogenase (LDH) enzymatic activity as an indicator of cell permeability using kits purchased from Roche (Indianapolis, IN, USA). The 96-well plates were centrifuged at 200*g* for 5 min to pellet uninternalized QDs. Supernatants (75 μL) were transferred to a clean plate, and LDH activity was assessed per the manufacturer's instructions. Cells treated with 0.1% Triton-100 serving as a positive control. QDs incubated with LDH reaction mix in a cell-free environment were used to determine if QDs caused assay interference. Reactions were read colormetrically on a BioTek plate reader at an absorbance wavelength of 490 nm and a reference wavelength of 600 nm after 15 min.

Mitochondrial activity, as measured using water-soluble tetrazolium dye (WST-1, Roche, Indianapolis, IN, USA), was assessed after incubation with QDs or 0.1% Triton-100 (positive control). WST-1 reagent was added to each well (7.5 μL) of 96-well plates; plates were briefly vortexed and then incubated at 37 °C and 5% CO_2 for 2−3 h prior to reading at an absorbance wavelength of 420 nm and a reference wavelength of 600 nm. QD suspensions were also incubated with the WST-1 reagent alone to determine potential assay interference. Experiments performed with MPA and CYST alone (no QDs) resulted in no cytotoxic responses (Supplemental Figure 5).

Oxidative Stress. Intracellular ROS formation in NHBE cells exposed to QDs was quantified using 5-(and-6)-carboxy-2′,-7′-dichlorodihydrofluorescein diacetate, acetyl ester (CM-H_2DCFDA, Molecular Probes, Eugene, OR, USA). NHBE cells exposed to DPBS only or 100 μmol/L H_2O_2 served as controls. QD controls at the highest concentrations were included in wells without cells to determine if QDs induce spontaneous fluorescence of CM-H_2DCFDA. Fluorescence was measured using an excitation wavelength of 490 nm and an emission wavelength of 535 nm every 10 min postexposure for 120 min. Readings beyond 120 min resulted in errant readings due to cell starvation. Representative data from the 60 min reading are presented.

DNA Damage. NHBE cells were exposed to QDs for 24 h, washed three times with DPBS, harvested by typsinization, counted, and resuspended at 2.5×10^5 cells per mL in freezing media consisting of 70% BEGM, 20% fetal bovine serum, and 10% dimethylsulfoxide (DMSO) prior to storage in liquid nitrogen until comet assay analyses. Cells treated with media only or exposed to 250 μmol/L H_2O_2 for 1 h served as controls for DNA strand breaks. DNA strand breaks were measured by alkaline comet assay, otherwise known as single cell gel electrophoresis (SCGE).[60] Low melting point agarose (300 μL, LMPA Agarose, Trevigen, Inc., MD, USA) was heated to 37 °C and combined with 30 μL of a $1-2 \times 10^5$ cells per mL cell suspension (ratio 1:10 volume fraction). Each well of a 20-well CometSlideTM (Trevigen, Inc., MD, USA) was filled with 30 μL of the cell/agarose suspension. The slides were placed in a 4 °C refrigerator in the dark for 15 min to solidify. Slides were then immersed in 50 mL of prechilled lysis solution (Trizma base, Triton X-100, DMSO, MD,USA) and left at 4 °C for 30−60 min to facilitate cell membrane and histone removal. After draining excess liquid, the slides were transferred to 50 mL of alkaline unwinding solution (200 mmol/L NaOH, 1 mmol/L EDTA, pH > 13) and incubated at room temperature in the dark for 20 min to denature and unwind DNA. After the unwinding step, electrophoresis was performed in the CometAssay ES tank (Trevigen, Inc., MD, USA) at 21 V for 30 min. Slides were then rinsed with distilled water and fixed with 70% ethanol. Slides were stained with SYBR Green I (Trevigen, Inc., MD, USA, 1:10000) and rinsed with distilled water to remove excess dye and minimize background staining. Slides were visualized by epifluorescence microscopy (Olympus System microscope, model BHT) equipped with the appropriate optical filter for SYBR Green I (excitation/emission spectrum, 460 and 560 nm, respectively, Chroma, 49002 ET GFP). Final magnification of the comet images was 100×. The images were recorded using a digital CCD camera (Photometrics, CoolSNAP HQ2) and were imported to an imaging analysis software (NIS Elements Nikon). The comet images were scored using CometScore software (Tritek, Corp., USA). DNA damage was reported as the percentage of DNA in the comet tail. For each sample (treated cells and controls), 30 comets per slide were analyzed in duplicate or triplicate, with two slides scored per sample. Approximately, 10 areas per slide were observed at five cells or less per field, taking care to avoid any selection bias, overlap counting of cells, and edge areas of slides. The percentage of DNA in the tail was calculated for each cell and averaged ($n = 30$ cells) for each treatment group. Percent DNA damage was determined as a function of treatment concentration and graphed as percent DNA in tail.

Immunocytochemistry. NHBE cells exposed to QDs for 6 or 24 h were evaluated for the presence of 53BP1 protein by first washing coverslips with DPBS, then fixing with 3% buffered formalin overnight at 4 °C. Coverslips were rinsed with DPBS and incubated with 25 mmol/L glycine for 5 min. Coverslips were again rinsed with DPBS then permeabilized with a solution of 0.4% Triton X-100 in DPBS for 5 min then blocked for 1 h in 0.1% bovine serum albumin (BSA). Coverslips were rinsed with NP40/BSA/PBS buffer and then with deionized H_2O. Coverslips were then incubated in a humidified chamber in the dark with mouse anti-human 53BP1 antibody (anti-53BP1 antibody, clone BP13, MAB3802, EMD Millipore Corp., MA, USA) at a concentration of 3 μg/mL in NP40/BSA/PBS buffer. Next, coverslips were again rinsed with NP40/BSA/PBS buffer and then with deionized H_2O. Alexa Fluor 488 goat anti-mouse IgG (Life Technologies, NY, USA) was diluted 1:300 in NP40/BSA/PBS buffer, added to coverslips, and incubated in a humidified chamber in the dark for 60 min. Coverslips were again rinsed with NP40/BSA/PBS buffer followed by two rinses with deionized H_2O. Nuclei were counterstained with Hoechst 33342 (Life Technologies, NY, USA) at a concentration of 1 μg/mL during the last dH_2O rinse. Cells were mounted on slides and visualized using a fluorescence microscope with a 40× objective (Zeiss Axiophot, Carl Zeiss, Germany) and imaged using Pro Plus software (Ver. 6.2, Media Cybernetics, MD, USA). Figure images are representative of at least three independent experiments.

Protein Isolation and Immunoblotting. NHBE cells were exposed to QDs for 24 h, and cytoplasmic extractions were isolated using NE-PER nuclear and cytoplasmic extraction reagents (Thermo Fisher Scientific, IL, USA) according to the manufacturers' protocol. Protein fractions were stored at −80 °C until analyses and immunoblotted as previously described.[61] Briefly, to analyze cytoplasmic p53, 50 μg of protein extract was heated to 95−100 °C for 5 min with Laemmli SDS sample buffer

(4×, Boston Bioproducts, MA, USA). Samples were separated by SDS polyacrylamide gel electrophoresis using a 12% gel with a 5% stacking gel using a mini-PROTEAN 3 cell system (Bio-Rad Laboratories, CA, USA). Following electrophoresis, proteins were transferred onto polyvinylidene difluoride membranes (0.45 μm; BioRad Laboratories, MA, USA). Nonspecific binding was blocked by incubating membranes in 5% (mass fraction) nonfat dry milk in Tris-buffered saline containing Tween 20 (TBS/T; 50 mmol/L Tris, pH 7.4, 150 mmol/L NaCl, and 0.1% (volume fraction) Tween 20) at room temperature for 1 h. Incubation was followed by three 5 min TBS/T washes; membranes were then incubated with a primary antibody (mouse anti-human p53, Immunotech, Beckman Coulter, CA, USA) suspended in 5% bovine serum albumin at a dilution of 1:1000 at 4 °C overnight. After washing with TBS/T, membranes were incubated with a horseradish peroxidase (HRP)-conjugated anti-mouse antibody (1:2000, Santa Cruz, CA, USA) for 1 h at room temperature. The protein bands were detected using a supersignal West Dura extended duration substrate (Thermo Scientific Pierce, IL, USA) and resolved on a BioRad ChemiDoc imaging system. The protein molecular weight was determined by comparison with Precision Plus protein prestained standards (Bio-Rad Laboratories, MA, USA). Blots were stripped using Restore Western Blot stripping buffer (Thermo Fisher Scientific, IL, USA) for 15 min and washed three times with TBS/T before reblocking and probing with mouse anti-human actin (1:1000, actin (ACTBD11B7) antibody: SC-81178, Santa Cruz, CA, USA) as a loading control.

RNA Isolation, High-Throughput Quantitative Polymerase Chain Reaction, and Transcriptomics. NHBE cells were exposed to 10 or 100 μg/mL MPA- or CYST-QDs for 6 h. Cells were washed three times with DPBS to remove residual QDs prior to lysis. RNA was harvested and purified using Qiagen RNeasy mini-prep kits (Valencia, CA, USA) per manufacturer's recommendations. For RNA samples used for transcriptomics, two DNA digestions were performed using Qiagen's RNase free DNase set (Valencia, CA, USA). The first DNA digestion was performed on the column for 40 min, and the second was performed prior to RNA cleanup for an additional 40 min. Gene expression changes for 96 targets were assessed using the BioMark real-time PCR high-throughput chip system and 96.96 dynamic arrays (Fluidigm, CA, USA). The 96 TaqMan assays tested in this report include regulatory genes for pathways including mitochondrial function, inflammation, DNA damage and repair, autophagy, and matrix formation. RNA quality was assessed and quantified using the Agilent 2100 BioAnalyzer RNA Nano chip system (Agilent Technologies, CA, USA) prior to further manipulation. First strand cDNA synthesis from 1 μg of RNA was achieved using high-capacity cDNA reverse transcription kits according to manufacturer's instructions (Life Technologies, NY, USA). To ensure expression studies for low abundance targets across 96 assays, cDNA was subjected to preamplification as outlined in ref 11. Upon completion of preamplification PCR, the products were diluted 1:5 with Tris-EDTA (TE) buffer and stored at −20 °C until real-time PCR analyses could be performed.

Quantitative PCR analyses were performed as previously described.[11] Briefly, a sample premix consisting of 2× TaqMan fast universal master mix (Life Technologies, NY, USA) and 20× GE sample loading reagent (Fluidigm, CA, USA) per sample was prepared; sample premix was then aliquoted into individual wells of a 96-well PCR plate. Next, preamplified sample cDNA was added to the plate containing sample premix. The plate was vortexed, centrifuged, and placed on ice until the chip loading. TaqMan gene expression assays were prepared in a separate individual 96-well PCR plate; each well contained equal amounts of a single 20× assay and 2× assay loading reagent (Fluidigm, CA, USA). Then, 96.96 dynamic array chips were primed using the preset protocol on the IFC Controller HX. The chip's inlets were then loaded according to manufacturer's instructions. After loading the chip, qPCR was performed on the BioMark instrument using BioMark HD data collection software v3.0.2. Data analyses were performed using Fluidigm real-time PCR analysis software. Sample ΔC_t values were calculated by using media-only values as the negative control. ΔC_t values were calculated for the TaqMan assays using β-actin as the normalizer reference gene. Significant changes in gene expression are reported as those genes whose expression was increased greater than 2-fold.

Global gene expression analysis was carried out using trancriptome sequencing (RNA-seq). Before using the RNA samples, the level of genomic DNA contamination was quantified with an 18S quantitative real-time PCR assay (Life Tech). Human DNA (NIST) was used as the quantity standard. Total RNA (5 μg) with insignificant amounts of contaminating genomic DNA was processed using the magnetic Ribo-Zero kit (human/mouse/rat, EpiCentre), which removes a large fraction of rRNA. The remaining RNA fraction, mostly consisting of mRNAs, was converted to directional Illumina sequencing libraries using the ScriptSeq kit (EpiCentre). All three samples were sequenced on one lane of Illumina HiSeq 2000.

For RNA sequencing, all the samples were sequenced on Illumina HiSeq 2000 platform (Illumina, CA). Altogether 107256140, 128846382, and 137929126 paired-end reads of 100 bp were generated for HCC-4, -5, and -6, respectively. Sequencing reads were mapped to human rRNA sequences in the UCSC annotated human genome (hg19) using Bowtie2.[62] The fractions of reads mapped to human rRNAs are 3.11, 7.23, and 3.40% for HCC-4, -5, and -6, respectively. All reads were mapped to the human genome (UCSC hg19) using Bowtie and Tophat.[62,63] About 70% of the total reads from each sample can be mapped to the human genome. The mapped reads were then assembled and quantified using Cufflinks.[64−66] To select significantly regulated genes with confidence, we defined a gene as significantly regulated if it had an adjusted p value (p-adj) less than 0.05. This adjusted p value helps to lower the identification of false positives and is considered a more stringent test compared to the traditional p value. Using p-adj with a threshold value of 0.05, a substantially lower number of signifcant gene regulation was noted, but those that are reported are of high confidence.

Statistical Analyses. Biological data are presented as fold change above or below the media control and graphically represented as mean fold change ± one standard deviation. Statistical significance was calculated by one-way analysis of variance (ANOVA) using multiple comparisons *versus* control group (Bonferroni t test). Analyses were performed using SigmaPlot version 11.0 (Systat Software, Inc., San Jose, CA, USA) using a minimum of three independent experiments for cell viability assays (LDH, mitochondrial function, and apoptosis). Numerical transformations of the data were performed as necessary to satisfy equivalence of variance and normality parameters before statistical analyses were conducted. Statistical significance for the 53BP1 foci immunocytochemistry was performed using the Mann−Whitney rank sum test. For the comet assays, statistical differences among treatment groups were evaluated by Student's t test. The p values <0.05 were considered statistically significant for all statistical analysis.

Conflict of Interest: The authors declare no competing financial interest.

Acknowledgment. We thank Cosby Lindquist for his assistance with figure presentation. We also thank Patrick Chain and Frances Hundley, members of Los Alamos National Laboratory's Genome Science group, a branch of the Department of Energy's Joint Genome Institute, for their excellence in transcriptomics. We are appreciative of Dr. Norman Doggett, Priya Dighe, and Melinda Wren of Los Alamos National Laboratory for the use of the BioMark high-throughput real-time PCR system. This work was supported by Los Alamos National Laboratory LDRD-DR program. This work was performed, in part, at the Center for Integrated Nanotechnologies, a U.S. Department of Energy, Office of Basic Energy Sciences user facility; J.A.H. also acknowledges partial support by NIH-NIGMS Grant 1R01GM084702-01. Los Alamos National Laboratory, an affirmative action equal opportunity employer, is operated by Los Alamos National Security, LLC, for the National Nuclear Security Administration of the U.S. Department of Energy under contract DE-AC52-06NA25396. Certain commercial equipment, instruments, and materials are identified in this paper to specify an experimental procedure as completely as possible. In no case does the identification of particular equipment or materials imply a

recommendation or endorsement by the National Institute of Standards and Technology nor does it imply that the materials, instruments, or equipment are necessarily the best available for the purpose.

Supporting Information Available: Supplemental methods, Supplemental Figure 1, 48 h necrosis of NHBE cells exposed to MPA-QDs; Supplemental Figure 2, micronuclei formation in QD-exposed cells; Supplemental Figure 3, corresponding 53BP1 nuclear staining; Supplemental Figure 4, ligand alone does not affect BP53 foci formation; Supplemental Figure 5, ligand alone does not cause cytotoxicity. Supplemental Table 1, calculations of cadmium loss from QDs in PBS buffers. Supplemental Table 2, cadmium leaching from negatively charged QDs with different ligands. Supplemental Table 3, list of gene targets used for high-throughput qPCR; Supplemental Table 4, transcriptome responses to MPA-QDs in NHBE cells; Supplemental Table 5, transcriptome responses to CYST-QDs in NHBE cells. This material is available free of charge *via* the Internet at http://pubs.acs.org.

REFERENCES AND NOTES

1. Pal, B. N.; Ghosh, Y.; Brovelli, S.; Laocharoensuk, R.; Klimov, V. I.; Hollingsworth, J. A.; Htoon, H. 'Giant' CdSe/CdS Core/Shell Nanocrystal Quantum Dots as Efficient Electroluminescent Materials: Strong Influence of Shell Thickness on Light-Emitting Diode Performance. *Nano Lett.* **2012**, *12*, 331–336.
2. Milliron, D. J.; Hughes, S. M.; Cui, Y.; Manna, L.; Li, J.; Wang, L.-W.; Paul Alivisatos, A. Colloidal Nanocrystal Heterostructures with Linear and Branched Topology. *Nature* **2004**, *430*, 190–195.
3. Mocatta, D.; Cohen, G.; Schattner, J.; Millo, O.; Rabani, E.; Banin, U. Heavily Doped Semiconductor Nanocrystal Quantum Dots. *Science* **2011**, *332*, 77–81.
4. Hu, M.; Yan, J.; He, Y.; Lu, H.; Weng, L.; Song, S.; Fan, C.; Wang, L. Ultrasensitive, Multiplexed Detection of Cancer Biomarkers Directly in Serum by Using a Quantum Dot-Based Microfluidic Protein Chip. *ACS Nano* **2010**, *4*, 488–494.
5. Diagaradjane, P.; Orenstein-Cardona, J. M.; Colón-Casasnovas, N. E.; Deorukhkar, A.; Shentu, S.; Kuno, N.; Schwartz, D. L.; Gelovani, J. G.; Krishnan, S. Imaging Epidermal Growth Factor Receptor Expression *in Vivo*: Pharmacokinetic and Biodistribution Characterization of a Bioconjugated Quantum Dot Nanoprobe. *Clin. Cancer Res.* **2008**, *14*, 731–741.
6. Walker, K.-A. D.; Morgan, C.; Doak, S. H.; Dunstan, P. R. Quantum Dots for Multiplexed Detection and Characterisation of Prostate Cancer Cells Using a Scanning Near-Field Optical Microscope. *PLoS ONE* **2012**, *7*, e31592.
7. Bagalkot, V.; Zhang, L.; Levy-Nissenbaum, E.; Jon, S.; Kantoff, P. W.; Langer, R.; Farokhzad, O. C. Quantum Dot−Aptamer Conjugates for Synchronous Cancer Imaging, Therapy, and Sensing of Drug Delivery Based on Bi-Fluorescence Resonance Energy Transfer. *Nano Lett.* **2007**, *7*, 3065–3070.
8. Muthu, M. S.; Kulkarni, S. A.; Raju, A.; Feng, S.-S. Theranostic Liposomes of TPGS Coating for Targeted Co-Delivery of Docetaxel and Quantum Dots. *Biomaterials* **2012**, *33*, 3494–3501.
9. Lovrić, J.; Bazzi, H. S.; Cuie, Y.; Fortin, G. R.; Winnik, F. M.; Maysinger, D. Differences in Subcellular Distribution and Toxicity of Green and Red Emitting CdTe Quantum Dots. *J. Mol. Med.* **2005**, *83*, 377.
10. Nagy, A.; Zane, A.; Cole, S. L.; Severance, M.; Dutta, P. K.; Waldman, W. J. Contrast of the Biological Activity of Negatively and Positively Charged Microwave Synthesized CdSe/ZnS Quantum Dots. *Chem. Res. Toxicol.* **2011**, *24*, 2176–2188.
11. Nagy, A.; Steinbrück, A.; Gao, J.; Doggett, N.; Hollingsworth, J. A.; Iyer, R. Comprehensive Analysis of the Effects of CdSe Quantum Dot Size, Surface Charge, and Functionalization on Primary Human Lung Cells. *ACS Nano* **2012**, *6*, 4748–4762.
12. Al-Hajaj, N. A.; Moquin, A.; Neibert, K. D.; Soliman, G. M.; Winnik, F. M.; Maysinger, D. Short Ligands Affect Modes of QD Uptake and Elimination in Human Cells. *ACS Nano* **2011**, *5*, 4909–4918.
13. Hoshino, A.; Fujioka, K.; Oku, T.; Suga, M.; Sasaki, Y. F.; Ohta, T.; Yasuhara, M.; Suzuki, K.; Yamamoto, K. Physicochemical Properties and Cellular Toxicity of Nanocrystal Quantum Dots Depend on Their Surface Modification. *Nano Lett.* **2004**, *4*, 2163–2169.
14. Hoshino, A.; Hanada, S.; Yamamoto, K. Toxicity of Nanocrystal Quantum Dots: The Relevance of Surface Modifications. *Arch. Toxicol.* **2011**, *85*, 707–720.
15. Kelf, T. A.; Sreenivasan, V. K.; Sun, J.; Kim, E. J.; Goldys, E. M.; Zvyagin, A. V. Non-specific Cellular Uptake of Surface-Functionalized Quantum Dots. *Nanotechnology* **2010**, *21*, 285105.
16. Nogueira, C.; Rocha, J. Toxicology and Pharmacology of Selenium: Emphasis on Synthetic Organoselenium Compounds. *Arch. Toxicol.* **2011**, *85*, 1313–1359.
17. Nordberg, G. F. Historical Perspectives on Cadmium Toxicology. *Toxicol. Appl. Pharmacol.* **2009**, *238*, 192–200.
18. Waalkes, M. P. Cadmium Carcinogenesis. *Mutat. Res., Fundam. Mol. Mech. Mutagen.* **2003**, *533*, 107–120.
19. Li, K. G.; Chen, J. T.; Bai, S. S.; Wen, X.; Song, S. Y.; Yu, Q.; Li, J.; Wang, Y. Q. Intracellular Oxidative Stress and Cadmium Ions Release Induce Cytotoxicity of Unmodified Cadmium Sulfide Quantum Dots. *Toxicol. in Vitro* **2009**, *23*, 1007–1013.
20. Derfus, A. M.; Chan, W. C. W.; Bhatia, S. N. Probing the Cytotoxicity of Semiconductor Quantum Dots. *Nano Lett.* **2004**, *4*, 11–18.
21. Kirchner, C.; Liedl, T. S.; Kudera, T.; Pellegrino, A.; Muñoz Javier, H. E.; Gaub, H. E.; Stölzle, S.; Fertig, N.; Parak, W. J. Cytotoxicity of Colloidal CdSe and CdSe/ZnS Nanoparticles. *Nano Lett.* **2005**, *5*, 331–338.
22. Lee, H. M.; Shin, D. M.; Song, H. M.; Yuk, J. M.; Lee, Z. W.; Lee, S. H.; Hwang, S. M.; Kim, J. M.; Lee, C. S.; Jo, E. K. Nanoparticles Up-Regulate Tumor Necrosis Factor-Alpha and CXCL8 *via* Reactive Oxygen Species and Mitogen-Activated Protein Kinase Activation. *Toxicol. Appl. Pharmacol.* **2009**, *238*, 160.
23. Lovrić, J.; Cho, S. J.; Winnik, F. M.; Maysinger, D. Unmodified Cadmium Telluride Quantum Dots Induce Reactive Oxygen Species Formation Leading to Multiple Organelle Damage and Cell Death. *Chem. Biol.* **2005**, *12*, 1227.
24. Foldbjerg, R.; Dang, D. A.; Autrup, H. Cytotoxicity and Genotoxicity of Silver Nanoparticles in the Human Lung Cancer Cell Line, A549. *Arch. Toxicol.* **2011**, *85*, 743–750.
25. Kim, H. R.; Kim, M. J.; Lee, S. Y.; Oh, S. M.; Chung, K. H. Genotoxic Effects of Silver Nanoparticles Stimulated by Oxidative Stress in Human Normal Bronchial Epithelial (BEAS-2B) Cells. *Mutat. Res., Fundam. Mol. Mech. Mutagen.* **2011**, *726*, 129–135.
26. Shukla, R. K.; Sharma, V.; Pandey, A. K.; Singh, S.; Sultana, S.; Dhawan, A. ROS-Mediated Genotoxicity Induced by Titanium Dioxide Nanoparticles in Human Epidermal Cells. *Toxicol. in Vitro* **2011**, *25*, 231–241.
27. Shukla, R. K.; Kumar, A.; Gurbani, D.; Pandey, A. K.; Singh, S.; Dhawan, A. TiO_2 Nanoparticles Induce Oxidative DNA Damage and Apoptosis in Human Liver Cells. *Nanotoxicology* **2011**, *7*, 48–60.
28. Jugan, M.-L.; Barillet, S.; Simon-Deckers, A.; Herlin-Boime, N.; Sauvaigo, S.; Douki, T.; Carriere, M. Titanium Dioxide Nanoparticles Exhibit Genotoxicity and Impair DNA Repair Activity in A549 Cells. *Nanotoxicology* **2011**, *6*, 501–513.
29. Khalil, W. K.; Girgis, E.; Emam, A. N.; Mohamed, M. B.; Rao, K. V. Genotoxicity Evaluation of Nanomaterials: DNA Damage, Micronuclei, and 8-Hydroxy-2-deoxyguanosine Induced by Magnetic Doped CdSe Quantum Dots in Male Mice. *Chem. Res. Toxicol.* **2011**, *24*, 640–650.
30. Jacobsen, N. R.; Møller, P.; Jensen, K. A.; Vogel, U.; Ladefoged, O.; Loft, S.; Wallin, H. Lung Inflammation and Genotoxicity Following Pulmonary Exposure to Nanoparticles in ApoE$^{-/-}$ Mice. *Part. Fibre Toxicol.* **2009**, *6*, 2.
31. Wang, L.; Zhang, J.; Zheng, Y.; Yang, J.; Zhang, Q.; Zhu, X. Bioeffects of CdTe Quantum Dots on Human Umbilical Vein Endothelial Cells. *J. Nanosci. Nanotechnol.* **2010**, *10*, 8591–8596.
32. Pala, I. R.; Arachchige, I. U.; Georgiev, D. G.; Brock, S. L. Reversible Gelation of II−VI Nanocrystals: The Nature of

Interparticle Bonding and the Origin of Nanocrystal Photochemical Instability. *Angew. Chem.* **2010**, *122*, 3743 –3747.
33. Aldana, J.; Wang, Y. A.; Peng, X. Photochemical Instability of CdSe Nanocrystals Coated by Hydrophilic Thiols. *J. Am. Chem. Soc.* **2001**, *123*, 8844–8850.
34. Dollefeld, H.; Hoppe, K.; Kolny, J.; Schilling, K.; Weller, H.; Eychmuller, A. Investigations on the Stability of Thiol Stabilized Semiconductor Nanoparticles. *Phys. Chem. Chem. Phys.* **2002**, *4*, 4747–4753.
35. Susumu, K.; Mei, B. C.; Mattoussi, H. Multifunctional Ligands Based on Dihydrolipoic Acid and Polyethylene Glycol To Promote Biocompatibility of Quantum Dots. *Nat. Protoc.* **2009**, *4*, 424–436.
36. Susumu, K.; Uyeda, H. T.; Medintz, I. L.; Pons, T.; Delehanty, J. B.; Mattoussi, H. Enhancing the Stability and Biological Functionalities of Quantum Dots *via* Compact Multifunctional Ligands. *J. Am. Chem. Soc.* **2007**, *129*, 13987–13996.
37. Lankoff, A.; Sandberg, W. J.; Wegierek-Ciuk, A.; Lisowska, H.; Refsnes, M.; Sartowska, B.; Schwarze, P. E.; Meczynska-Wielgosz, S.; Wojewodzka, M.; Kruszewski, M. The Effect of Agglomeration State of Silver and Titanium Dioxide Nanoparticles on Cellular Response of HepG2, A549 and THP-1 Cells. *Toxicol. Lett.* **2012**, *208*, 197–213.
38. Yan, M.; Zhang, Y.; Xu, K.; Fu, T.; Qin, H.; Zheng, X. An *In Vitro* Study of Vascular Endothelial Toxicity of CdTe Quantum Dots. *Toxicology* **2011**, *282*, 94–103.
39. Faux, S. P.; Tai, T.; Thorne, D.; Xu, Y.; Breheny, D.; Gaca, M. The Role of Oxidative Stress in the Biological Responses of Lung Epithelial Cells to Cigarette Smoke. *Biomarkers* **2009**, *14* (Suppl 1), 90–96.
40. Shih, R. S.; Wong, S. H.; Schoene, N. W.; Lei, K. Y. Suppression of GADD45 Alleviates the G2/M Blockage and the Enhanced Phosphorylation of p53 and p38 in Zinc Supplemented Normal Human Bronchial Epithelial Cells. *Exp. Biol. Med.* **2008**, *233*, 317–327.
41. Ricks-Santi, L. J.; Sucheston, L. E.; Yang, Y.; Freudenheim, J. L.; Isaacs, C. J.; Schwartz, M. D.; Dumitrescu, R. G.; Marian, C.; Nie, J.; Vito, D.; *et al.* Association of Rad51 Polymorphism with DNA Repair in BRCA1Mutation Carriers and Sporadic Breast Cancer Risk. *BMC Cancer* **2011**, *11*, 278.
42. Beger, C.; Ramadani, M.; Meyer, S.; Leder, G.; Krüger, M.; Welte, K.; Gansauge, F.; Beger, H. G. Down-Regulation of BRCA1 in Chronic Pancreatitis and Sporadic Pancreatic Adenocarcinoma. *Clin. Cancer Res.* **2004**, *10*, 3780–3787.
43. Chabalier, C.; Lamare, C.; Racca, C.; Privat, M.; Valette, A.; Larminat, F. BRCA1 Downregulation Leads to Premature Inactivation of Spindle Checkpoint and Confers Paclitaxel Resistance. *Cell Cycle* **2006**, *5*, 1001–1007.
44. Deng, C. X. BRCA1: Cell Cycle Checkpoint, Genetic Instability, DNA Damage Response and Cancer Evolution. *Nucleic Acids Res.* **2006**, *34*, 1416–1426.
45. Badie, C.; Itzhaki, J. E.; Sullivan, M. J.; Carpenter, A. J.; Porter, A. C. Repression of CDK1 and Other Genes with CDE and CHR Promoter Elements during DNA Damage-Induced G(2)/M Arrest in Human Cells. *Mol. Cell. Biol.* **2000**, *20*, 2358–2366.
46. Noon, A. T.; Goodarzi, A. A. 53BP1-Mediated DNA Double Strand Break Repair: Insert Bad Pun Here. *DNA Repair* **2011**, *10*, 1071–1076.
47. Sutter, T. R.; Tang, Y. M.; Hayes, C. L.; Wo, Y. Y.; Jabs, E. W.; Li, X.; Yin, H.; Cody, C. W.; Greenlee, W. F. Complete cDNA Sequence of a Human Dioxin-Inducible mRNA Identifies a New Gene Subfamily of Cytochrome P450 that Maps to Chromosome 2. *J. Biol. Chem.* **1994**, *269*, 13092–13099.
48. Omura, T.; Sato, R. The Carbon Monoxide-Binding Pigment of Liver Microsomes. I. Evidence for Its Hemoprotein Nature. *J. Biol. Chem.* **1964**, *239*, 2370–2378.
49. Hayes, C. L.; Spink, D. C.; Spink, B. C.; Cao, J. Q.; Walker, N. J.; Sutter, T. R. 17-β Estradiol Hydroxylation Catalyzed by Human Cytochrome P450 1B1. *Proc. Natl. Acad. Sci. U.S. A.* **1996**, *93*, 9776–9781.
50. McKenna, I. M.; Gordon, T.; Chen, L. C.; Anver, M. R.; Waalkes, M. P. Expression of Metallothionein Protein in the Lungs of Wistar Rats and C57 and DBA Mice Exposed to Cadmium Oxide Fumes. *Toxicol. Appl. Pharmacol.* **1998**, *153*, 169–178.
51. Wicherek, L.; Dutsch-Wicherek, M.; Galazka, K.; Banas, T.; Popiela, T.; Lazar, A.; Kleinrok-Podsiadlo, B. Comparison of RCAS1 and Metallothionein Expression and the Presence and Activity of Immune Cells in Human Ovarian and Abdominal Wall Endometriomas. *Reprod. Biol. Endocrinol.* **2006**, *4*, 41.
52. King-Heiden, T. C.; Wiecinski, P. N.; Mangham, A. N.; Metz, K. M.; Nesbit, D.; Pedersen, J. A.; Hamers, R. J.; Heideman, W.; Peterson, R. E. Quantum Dot Nanotoxicity Assessment Using the Zebrafish Embryo. *Environ. Sci. Technol.* **2009**, *43*, 1605–1611.
53. George, S.; Xia, T.; Rallo, R.; Zhao, Y.; Ji, Z.; Lin, S.; Wang, X.; Zhang, H.; France, B.; Schoenfeld, D.; *et al.* Use of a High-Throughput Screening Approach Coupled with *In Vivo* Zebrafish Embryo Screening To Develop Hazard Ranking for Engineered Nanomaterials. *ACS Nano* **2011**, *5*, 1805–1817.
54. Oberdorster, G.; Cherian, M. G.; Baggs, R. B. Correlation between Cadmium-Induced Pulmonary Carcinogenicity, Metallothionein, and Inflammatory Processes: A Species Comparison. *Environ. Health Perspect.* **1994**, *102*, 257–263.
55. Ho, C.-C.; Chang, H.; Tsai, H.-T.; Tsai, M.-H.; Yang, C.-S.; Ling, Y.-C.; Lin, P. Quantum Dot 705, a Cadmium-Based Nanoparticle, Induces Persistent Inflammation and Granuloma Formation in the Mouse Lung. *Nanotoxicology* **2011**, *7*, 105–115.
56. Ma-Hock, L.; Brill, S.; Wohlleben, W.; Farias, P. M. A.; Chaves, C. R.; Tenório, D. P. L. A.; Fontes, A.; Santos, B. S.; Landsiedel, R.; Strauss, V.; *et al.* Short Term Inhalation Toxicity of a Liquid Aerosol of CdS/Cd(OH)$_2$ Core Shell Quantum Dots in Male Wistar Rats. *Toxicol. Lett.* **2012**, *208*, 115–124.
57. Chau, E.; Galloway, J. F.; Nelson, A.; Breysse, P. N.; Wirtz, D.; Searson, P. C.; Sidhaye, V. K. Effect of Modifying Quantum Dot Surface Charge on Airway Epithelial Cell Uptake *in Vitro*. *Nanotoxicology* **2012**, *7*, 1143–1151.
58. Mahler, B.; Lequeux, N.; Dubertret, B. T. Ligand-Controlled Polytypism of Thick-Shell CdSe/CdS Nanocrystals. *J. Am. Chem. Soc.* **2009**, *132*, 953–959.
59. Yu, W. W.; Qu, L.; Guo, W.; Peng, X. Experimental Determination of the Extinction Coefficient of CdTe, CdSe, and CdS Nanocrystals. *Chem. Mater.* **2003**, *15*, 2854–2860.
60. Petersen, E. J.; Nelson, B. C. Mechanisms and Measurements of Nanomaterial-Induced Oxidative Damage to DNA. *Anal. Bioanal. Chem.* **2010**, *398*, 613–650.
61. Gao, J.; Wang, H. L.; Shreve, A.; Iyer, R. Fullerene Derivatives Induce Premature Senescence: A New Toxicity Paradigm or Novel Biomedical Applications. *Toxicol. Appl. Pharmacol.* **2010**, *244*, 130–143.
62. Langmead, B.; Trapnell, C.; Pop, M.; Salzberg, S. L. Ultrafast and Memory-Efficient Alignment of Short DNA Sequences to the Human Genome. *Genome Biol.* **2009**, 10.
63. Roberts, A.; Trapnell, C.; Donaghey, J.; Rinn, J. L.; Pachter, L. Improving RNA-Seq Expression Estimates by Correcting for Fragment Bias. *Genome Biol.* **2011**, *12*, R22.
64. Roberts, A.; Pimentel, H.; Trapnell, C.; Pachter, L. Identification of Novel Transcripts in Aannotated Genomes Using RNA-Seq. *Bioinformatics* **2011**, *27*, 2325–2329.
65. Trapnell, C.; Roberts, A.; Goff, L.; Pertea, G.; Kim, D.; Kelley, D. R.; Pimentel, H.; Salzberg, S. L.; Rinn, J. L.; Pachter, L. Differential Gene and Transcript Expression Analysis of RNA-Seq Experiments with TopHat and Cufflinks. *Nat. Protoc.* **2012**, *7*, 562–578.
66. Trapnell, C.; Williams, B. A.; Pertea, G.; Mortazavi, A.; Kwan, G.; Van Baren, M. J.; Salzberg, S. L.; Wold, B. J.; Pachter, L. Transcript Assembly and Quantification by RNA-Seq Reveals Unannotated Transcripts and Isoform Switching during Cell Differentiation. *Nat. Biotechnol.* **2010**, *28*, 516–520.